A Ballistic Projectile Tracking System using Continuous Wave Doppler Radar

J.D. Pinezich[1], Jason Heller[2], Ting Lu[3]

[1]Adv. Acoustic Concepts Inc., [2]Applied Math. and Stat., Stony Brook University, [3]Elec. and Comp. Eng., Stony Brook University

Abstract— **We present in this paper the theory of operation, together with experimental results, of a projectile target scoring system that determines highly accurate hit locations of small arms fire by processing CW-radar Doppler phase content into a trajectory estimate. We describe a new algorithm for extracting trajectory parameters from Doppler time series to obtain time, distance, and velocity at closest approach. Vector trajectories are derived by combining multiple scalar trajectories from three radar units. Live fire test results from a local range and Aberdeen Proving Ground are provided to show that a hit location accuracy of 4 cm can be achieved reliably on small arms.**

Keywords— **CW-radar, Doppler phase, ballistics, trajectory estimation.**

I. Introduction

THERE is a growing need for accurate and affordable instrumentation to meet the demands of testing new weapons systems and training soldiers to use new weapons. Present day scoring systems include electro-optical (spark photography, laser grid) and optical (high speed video) systems [1] which are expensive and difficult to calibrate. Also in use are acoustic systems that detect shocks and determine hit location parameters with triangulation [2]; these are useful only for projectiles with supersonic velocity. Since most projectiles carry charge, methods have also been proposed that locate by measuring electric field [8]. Most promising are radar systems due to their robustness, portability, accuracy and near real-time operation. Pulse-Doppler systems have resolution limitations due to pulse-width (Cartwright-NCHS 15 cm accuracy), while ultra-wideband impulse radars suffer from interference (Cambridge Consultants AN/DSQ-57). We have developed an algorithm based on continuous wave (CW) radar, and built and tested a system with superior performance on small arms projectiles including 25 mm rounds and 40 mm grenades.

This work is part of an ongoing project, Doppler Advanced Radar Target Scoring (DARTS), with Aberdeen Test Center (ATC) at Aberdeen Proving Ground (APG). The results here were collected using a development system consisting of three sensors manufactured as part of the feasibility studies for a production system at APG, see figure 1. A total of 17 production units are scheduled for installation at ATC's Evasive Target Warfare (ETW) range, providing scoring for an area 10 meters high and 80 meters wide.

CW systems are highly attractive due to their simplicity and are extensively used at proving grounds for projectile velocity estimation (Weibel Scientific). While CW-radar is well established for velocity estimation, its application to range estimation requires apriori assumptions on the target motion. For example, Weibel radars are typically mounted near the muzzle with muzzle-offset surveyed, have pencil-beam antenna patterns pointing downrange, and have a trigger indicating time of fire. Distance traveled is calculated by integrating velocity. More complex is constant velocity linear motion with unknown time, distance and velocity at closest approach. A number of authors have presented interesting algorithms based on this approximation. Levanon [3] expands time-varying Doppler $f(t)$ in a Taylor series and shows that $(f, \dot{f}, \ddot{f})$ at a single point in time can be inverted to yield range and velocity magnitudes and the angle between the corresponding vectors. Webster [4] points out that Levanon's approach introduces a bias due to truncation of the Taylor series; he formulates an algebraic solution in terms of three sequential Doppler estimates $f(0), f(\tau), f(2\tau)$. Numerical experiments have shown that these methods are susceptible to both noise and frequency smearing. Levanon and Weinstein [5] present a potentially useful algorithm for computing the velocity parameter directly from Doppler phase. In the area of combining multiple radar estimates, Allen and Stoughton [6] propose a system that converts distance, velocity, and time

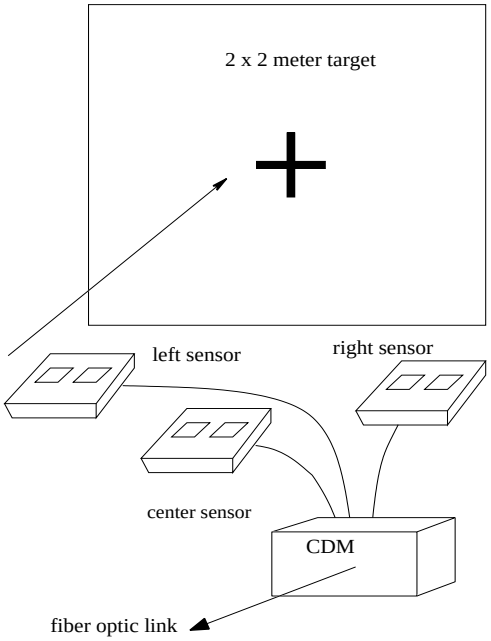

Fig. 1. System configuration. Sensors form triangle in the horizontal plane.

at closest approach to three radars into direction of arrival. Armstrong and Holeman present an algorithm of parameter estimation for a constant-acceleration motion model using nonlinear optimization [7]. A difficulty with this method is that it requires a fairly accurate initial guess to find the optimal solution, and is computationally expensive. However, he presents experimental results that show accuracies on the order of 3 cm for estimation of hit location of a pitched baseball.

We propose what we believe is a novel iterative data-transformation method, with high accuracy and computational speed, that uses linear curve fitting over the entire set of available data. Although the estimation problem is inherently non-linear, the assumption of a constant-velocity straight-line trajectory allows it to be linearized via the data transformation technique. Since observation times are short, the straight-line assumption is generally valid; however, over the intervals of interest the trajectories are not well approximated by constant velocity methods. Instead we use an exponential velocity model based on constant retardation. This method was motivated by analyis of previous methods based on processing Doppler frequency [3], [4] in which it was observed that (1) frequency estimation was poor due to smearing; (2) significant Doppler content was not used in the trajectory estimate. Our approach avoids the need to estimate frequency directly and combines all available information since it uses phase. Moreover, by restricting the initial processing to scalar trajectories we gain accuracy and speed advantages through linearization via the data transformation method.

From experimental results, distance errors are less than 4 cm at distances up to 2 m. Recent preliminary testing on the ETW system indicates similar performance out to at least 8 m with similarly specified hardware. Many factors contribute to errors, including noise, multipath, antenna pattern anomolies, antenna survey error, projectile retardation, projectile geometry and instability. Although an error budget analysis of the magnitudes of these contributions would be valuable, we have not attempted to do this.

The remainder of this paper is organized as follows: in Section II, we describe the system design. In Section III, we present the ballistic trajectory algorithm. In Section IV, live fire testing results are provided to demonstrate the performance of our system. Finally, Section V contains the conclusions and future work. The authors would like to acknowledge the work of Tien Nguyen of Aberdeen Test Center, and Dave Owen and Denny Nembhard of Target Systems Technologies for building the hardware.

II. SYSTEM DESCRIPTION

The scoring system layout is pictured in figure 1. Each homodyne sensor downconverts the received echo using the transmit waveform as the local oscillator, so that the receiver output is the Doppler shifted return amplitude modulated by radar range and antenna beam. Down-range equipment consists of radar sensors and a controller/data-multiplexer (CDM). Frequencies are nominally 10 MHz apart, tunable in a band from 5.6 to 5.8 GHz. Each sensor consists of a pair of patch antennas for receive and transmit, with transceiver electronics mounted to the back of the antenna ground plate. The source is a dielectric resonant oscillator driving a +33 dBm amplifier, the receiver has a low noise front-end, filtering, and a 10-bit A/D converter sampled at 1.8 MHz, see figure 2. The antenna design was chosen for its broad beam radiation pattern, important for maximizing capture of incoming Doppler shifted signal, and good isolation needed to suppress oscillator phase noise.

The sensors are grouped together in sets of three. This allows for the CDM to pack a single 4 byte word with three 10-bit data words from a sensor triad. For ETW, the CDM will support up to 24 sensors in 8 channels. A master clock generated in the CDM forms the common trigger for the A/D converter in each sensor, thus the system is fully synchronous. Data collected and formatted by the CDM is transmitted over fiber optic link to the uprange PC. The uprange PC provides for Doppler data storage and control of the downrange equipment. The data analysis presented here was done offline. Processing time for a single shot is less than 10 seconds. The software is written in C.

III. SCORING ALGORITHM

A. Overview

Individual sensors produce independent scalar trajectory estimates; multiple scalar trajectories are combined to estimate true trajectory. Scalar algorithm geometry is shown in figure 3. The trajectory model assumes the projectile is traveling in a straight line with velocity $V(t)$ governed by constant retardation, *i.e.* exponential decay. Projectile range $R(t)$ has four parameters: distance d_{ca}, time t_{ca}, and velocity v_{ca} at closest approach, and retardation K. The system is assumed monostatic with phase center at the midpoint between the two antenna patches.

The basic estimation algorithm is a three step process that assumes retardation is zero: 1) convert received Doppler into phase, 2) convert phase into range, and 3) convert range into scalar trajectory parameters d_{ca}, t_{ca}, v_{ca}. For each sensor these steps are carried out twice: first without compensation for retardation (coarse estimate); second with adjusted times which compensate for retardation (fine estimate), see figure 4.

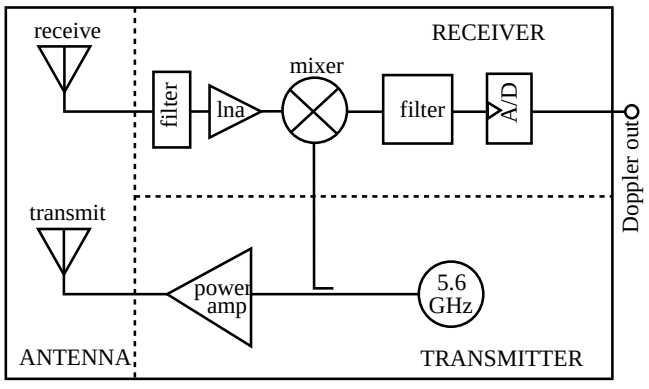

Fig. 2. CW radar transceiver block diagram.

B. Constant Velocity Scoring Algorithm

The phase history of the radar return is proportional to the projectile range to the radar and encodes the parameters of the trajectory. This can be seen in the received Doppler signal $F(t) = A(t)\cos\Phi(t)$, obtained by mixing the radar return with the transmitted signal:

$$\Phi(t) = 2\pi\frac{2R(t)}{\lambda} = 4\pi\frac{\sqrt{v_{ca}^2(t-t_{ca})^2 + d_{ca}^2}}{\lambda}, \qquad (1)$$

where λ is the transmit wavelength. A typical Doppler signal is shown in figure 5.

Phase can be extracted from $F(t)$ relative to phase at some time τ_0; the resulting phase history is proportional to relative range $Q(t) = R(t) - R(\tau_0)$. We use two fairly robust methods for phase extraction: detection of zero-crossings and detection of inflection points. For pure sinusoids, zero-crossings and inflection points coincide and occur twice per period. Amplitude and phase modulation and noise can introduce extraneous points of both types. We have found that for high frequencies, inflection point detection is more robust with lower phase noise output, while at low frequencies the zero-crossings are more robust. In particular, at low frequencies several phenomena occur: phase reversal at closest approach, high-pass filtering for clutter rejection, and amplitude saturation in the A/D converter, all causing extraneous inflection points at low frequency.

For zero crossings we use linear interpolation to find times τ where $F(\tau) = 0$; for inflection points we use cubic interpolation. Let $\tau_i, i = 0, ..., N$ be consecutive times for detected phase markers, with $\tau_N < t_{ca}$, and for each i put $Q_i = -i\lambda/4$. Phase points at times after t_{ca} are not included for the following reasons: antenna beams point toward the firing position and negative Doppler is not captured reliably; projectile tail returns are asymmetric with respect to nose returns resulting in unknown phase shift for all but the smallest projectiles; for physical targets, projectile impact violates the constant-velocity straight-line trajectory assumption. A first estimate of t_{ca} is obtained by detecting the maximum amplitude in the autoconvolution of the Doppler data. A relative range curve for the data of figure 5 is shown in figure 6(a).

Conversion of relative range to true range requires determination of $R(\tau_0)$, the range at the first phase point. Let

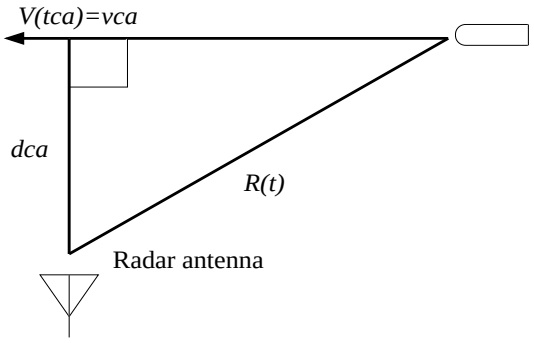

Fig. 3. Geometry of scalar scoring system.

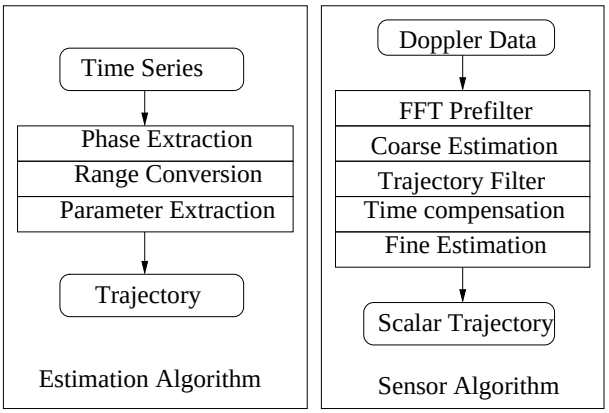

Fig. 4. Coarse and fine estimation (right) uses the basic estimation algorithm (left).

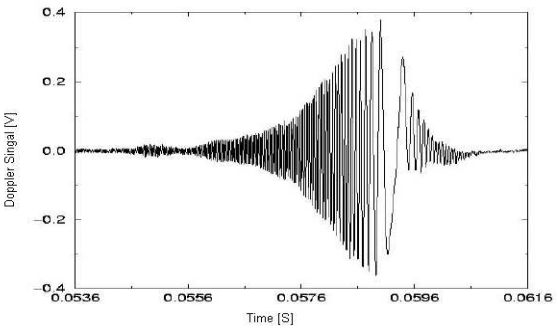

Fig. 5. Received Doppler signal taken from local range test. The projectile was 5.56 mm, approximate trajectory: $d_{ca} = 1.35$ m, $t_{ca} = 59.23$ ms, $v_{ca} = 902.7$ m/s.

R^* be an estimate for $R(\tau_0)$ and for each i compute

$$\begin{aligned} W_i &= (Q_i + R^*)^2 \\ &= (\sqrt{(v_{ca}(\tau_i - t_{ca}))^2 + d_{ca}^2} - R(\tau_0) + R^*)^2 \\ &= v_{ca}^2(\tau_i - t_{ca})^2 + d_{ca}^2 + 2\Delta R(\tau_i) + \Delta^2, \end{aligned}$$

where $\Delta = R^* - R(\tau_0)$. For $\Delta = 0$ the values W_i are related to the times τ_i by a quadratic polynomial, conversely when $\Delta \neq 0$ the points are *not* described by a quadratic since $R(t)$ is hyperbolic. It follows that the least squares error of a quadratic curve fit to the transformed data (τ_i, W_i) is minimized when $R^* = R(\tau_0)$, allowing the true range to be computed, see figure 6(b).

We use Newton iterations to converge to the best estimate of $R(\tau_0)$ yielding polynomial $at^2 + bt + c$. The coefficients are given by $[a, b, c]^t = (T^tT)^{-1}T^tW$ where the rows of matrix T are given by $[\tau_i^2, \tau_i, 1]$, $i = 0, 1, ..., N$ and $W = [W_0, W_1, ..., W_N]^t$ is computed using the optimal R^*. Trajectory parameters t_{ca}, d_{ca}, v_{ca} are then given by:

$$v_{ca} = \sqrt{a} \qquad t_{ca} = -\frac{b}{2a} \qquad d_{ca} = \sqrt{c - \frac{b^2}{4a}} \qquad (2)$$

C. Trajectory Based Filter

Due to the radar inverse power law and antenna beam limitations, Doppler data captured at the beginning of an

acquisition cycle is dominated by thermal noise. Accurate trajectory estimates depend strongly on the Doppler extent used for the curve fitting, and since Doppler frequency sweeps from $2v(t)/\lambda$ down to DC, bandpass filtering is not sufficient to render subnoise Doppler information useful. Given a trajectory estimate, projectile range is synthesized and used to generate an in-phase and a quadrature estimate of the received Doppler waveform. These are mixed with the Doppler, filtered at (typically) 1 kHz, and upconverted back to Doppler frequencies. See figure 7. This effectively synthesizes a narrowband filter with center frequency that sweeps synchronously with the Doppler.

The performance of the trajectory based filter is shown in figure 8. We have found that a relatively poor trajectory estimate is sufficient to considerably improve the SNR of the waveform. Two issues of potential concern are when the Doppler signal has components at less than half the lowpass filter cutoff frequency so that sum as well as difference frequencies are passed through, and the leakage level of the original estimate into the filtered output. Leakage levels are generally much lower than signal levels; however when the original trajectory estimate is poor the filter can reject the true signal and subsequent trajectory estimates can be based on the leakage signal.

D. Retardation

The constant velocity assumption required by the basic estimation algorithm is not valid for realistic trajectories due to deceleration by drag forces. To obtain an improved estimate, a constant retardation velocity profile is assumed. According to [9] a constant retardation velocity model can well describe the motion of the projectile, especially over short distances, *e.g.* 10 meters. Thus we assume

$$V(t) = v_{ca} \cdot \exp\big(-K \cdot (t - t_{ca})\big). \tag{3}$$

We employ retardation compensation to map the relative range data into a constant velocity trajectory. Reasonably good estimates for t_{ca} and K are required to form the map, in which time values τ_i of relative range pairs (τ_i, Q_i) are adjusted to τ_i', based on constant velocity v_{ca}. Let x_i be the distance to the point of closest approach at time τ_i:

$$x_i = v_{ca} \int_{t_{ca}}^{\tau_i} \exp\big(-K(t - t_{ca})\big)\,\mathrm{dt}. \tag{4}$$

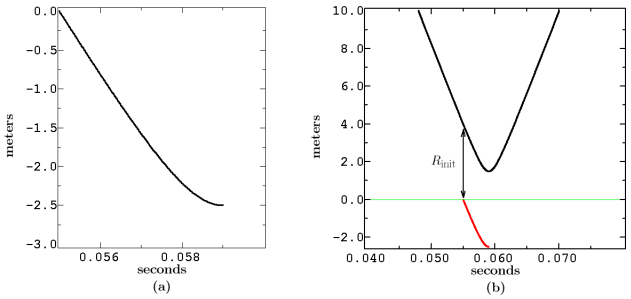

Fig. 6. (a) Relative range for the data of figure 5; range at initial detection is set to zero resulting in negative values as projectile nears. (b) Relative range (bottom curve) shown with extrapolated true range estimate (top curve).

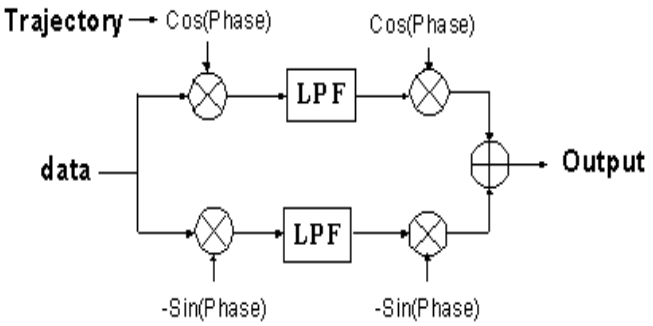

Fig. 7. Structure of trajectory based filter

Then a constant velocity profile that compensates for retardation is obtained by setting for each i:

$$\tau_i' = t_{ca} + \frac{x_i}{v_{ca}}. \tag{5}$$

E. Scalar Algorithm

The scalar algorithm is diagrammed in figure 4. The coarse estimate is obtained using no retardation compensation, an estimate of t_{ca} from Doppler data autoconvolution, and a fixed time window $[t_{ca} - T_b, t_{ca}]$ of relative range data, dependent on bullet type. The resulting trajectory estimate is used for trajectory-based filtering of the Doppler data and a new relative range curve is extracted. Retardation compensation is applied using the coarse estimate t_{ca} and an estimate of retardation. Using a new time window with width T_b' the fine trajectory estimate is computed and output as the scalar trajectory for the round.

Currently there are three methods of estimating retardation: bullet-type, Weibel radar, and internal estimate. For bullet type, a retardation value is assigned for each type. Retardation depends on projectile shape, size, and velocity, and on ambient conditions. For a practical system, a retardation model dependent based on experimental results would be queried using the uncompensated data trajectory estimate. Velocity and retardation values are standard Weibel outputs and are considered highly accurate. When available, Weibel retardation values are the

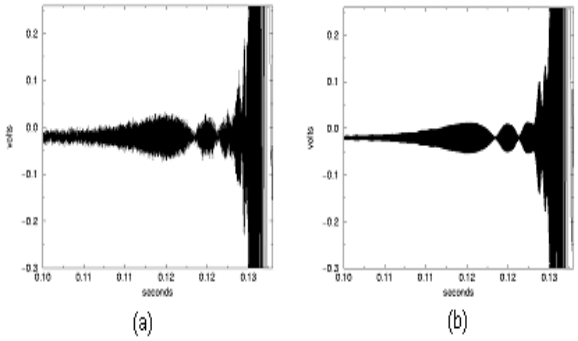

Fig. 8. (a) 120 mm round Doppler; (b) Output of trajectory-based filter

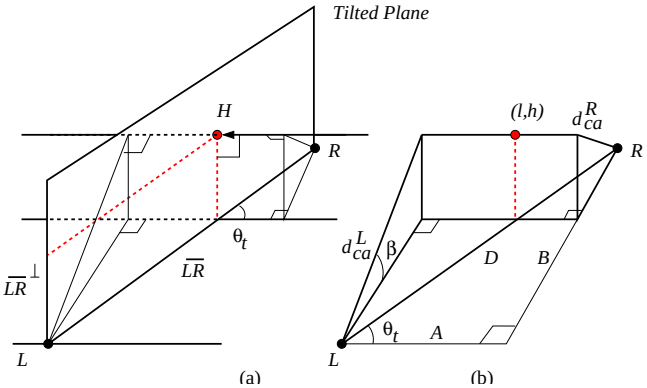

Fig. 9. (a) Geometry of 2D scoring. (b) Pertaining to the calculation of (l, h).

most accurate, however for small projectiles fired at great distances (e.g. 50 cal at 1000 m), Weibel does not always fully track. The desired solution to the retardation problem is an internally generated estimate based on Doppler data. Several such algorithms have been tested but with errors that exceed the tabulation by bullet-type method.

F. 2D Trajectory

Scalar trajectory information generated independently by two radar sensors (*e.g.* left and right) is combined to give the hit location (l, h) in a plane determined by the radar coordinates and trajectory elevation angle, see figure 9. This tilted plane is defined by the locations L and R of the two radars, and the projectile point of closest approach H to the the radar-pair axis of symmetry $\overline{LR}$. It has local coordinate system with origin at L and axes $\overline{LR}$ and $\overline{LR}^{\perp}$. The tilt angle γ is the rotation of the tilted plane about the radar axis with $\gamma = 0$ corresponding to a vertical plane. Relative to this plane and the radar-pair axis the trajectory's apparent azimuth angle is denoted θ_t. The apparent elevation angle is zero by definition. The coordinates of H in the tilted plane coordinate system are (l, h).

The distance A traveled between the points corresponding to closest approach to each radar is given by

$$A = \int_{t_{ca}^R}^{t_{ca}^L} V(t)\,\mathrm{d}t \tag{6}$$

where the superscript L, R refer to left and right radar trajectories respectively, and $V(t)$ is obtained as an average of left and right velocity estimates. This gives angle θ_t and triangle base length B:

$$\theta_t = \arcsin\left(\frac{A}{D}\right) \qquad B = D\cos\theta_t, \tag{7}$$

where $D = \|R - L\|$. The triangle with vertices L, R, and H, projected onto the trajectory orthogonal plane, has sides of lengths B, d_{ca}^R, and d_{ca}^L from which angle β can be found:

$$\cos\beta = \frac{{d_{ca}^L}^2 + B^2 - {d_{ca}^R}^2}{2Bd_{ca}^L}. \tag{8}$$

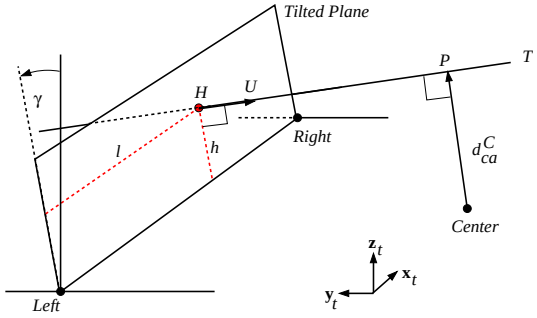

Fig. 10. Geometry for combining a 2D trajectory and a scalar trajectory into a 3D trajectory.

The hit location coordinates (l, h) are then given by

$$l = \frac{d_{ca}^L \cos\beta}{\cos\theta_t} \qquad h = d_{ca}^L \sin\beta. \tag{9}$$

G. 3D Trajectory

For horizontal trajectories, the tilted plane and the target plane are both vertical, and good hit location estimates can be computed using just two radars. However, in general it is necessary to determine tilt angle γ, so that the tilted plane can be mapped to the target plane. The 2D trajectory determines a circle of radius h orthogonal to the $\overline{LR}$ axis, centered at l along it; this circle contains the point H. The actual trajectory T passes through H with direction U. Given L, R, l, h and any tilt angle γ, an estimate of H can be resolved in three dimensions, and using it and θ_t an estimate of U can be resolved. The estimates for H and U are used to derive an estimate of d_{ca}^C, which we compare to the value reported by the center scalar trajectory.

Let γ^* be an estimate for γ resulting in estimates H^* for H and U^* for U. Let $\mathbf{x}_t, \mathbf{y}_t, \mathbf{z}_t$ be unit vectors in a right handed coordinate system such that $\mathbf{x}_t$ is in direction $\overline{LR}$ and $\mathbf{y}_t$ is horizontal in the downrange direction, see figure 10. Note that $\mathbf{x}_t, \mathbf{y}_t, \mathbf{z}_t$ are easily derived in a global coordinate system (e.g. from range geodetic survey) once L and R are given in that system. With U directed from H to P, we have

$$H^* = l\,\mathbf{x}_t + h\sin\gamma^*\,\mathbf{y}_t + h\cos\gamma^*\,\mathbf{z}_t, \tag{10}$$

$$U^* = \sin\theta_t\,\mathbf{x}_t - \cos\theta_t\cos\gamma^*\,\mathbf{y}_t + \cos\theta_t\sin\gamma^*\,\mathbf{z}_t. \tag{11}$$

We estimate T by constructing a line T^* that passes through H^* in direction U^*. Along T^* is a unique point P^* that is the point of closest approach to the center radar at C. Let $d(\gamma^*) = \|P^* - C\|$. Then if $d(\gamma^*) = d_{ca}^C$, $\gamma^* = \gamma$. This final equation

$$\sqrt{\|H^* - C\|^2 - \|(H^* - C)\cdot U^*\|^2} = d_{ca}^C \tag{12}$$

is solved numerically using Newton iterations.

IV. EXPERIMENTAL RESULTS

Shown below are results of live fire tests conducted on the DARTS system at two venues: a local firing range and Aberdeen Proving Ground. Small arms testing on the scalar

system was initially conducted on a variety of projectile types including 223 Remington, 44 Magnum, 357 Magnum, 45 Automatic, shotgun slug, and others, covering a wide range of projectile sizes and velocities. Results from these experiments were very encouraging and resulted in hardware and algorithmic improvements, ultimately producing accuracies better than 4 cm mean square radial error. At Aberdeen Proving Ground, data was collected from 5.56 mm rifle, 9 mm, 25 mm rounds, 40 mm rounds. Truth data for the shots reported below was determined by hand measuring impact hole locations in the target plywood. Weibel radar data was used to determine retardation per round type. The numbers presented have not been calibrated to eliminate bias. For each session of testing all shots that resulted in both valid data files and truth data are listed. In some cases data was not collected due to missed triggers and for other cases the projectile failed to hit the target so there was no truth data.

V. CONCLUSIONS

The results indicate that a hit location accuracy of 4 cm or better can be achieved reliably by the DARTS system. Constructed with a simple homodyne receiver design, such a system can provide real time trajectory scores for a wide range of projectiles by using the proposed ballistic estimation algorithm. An operational and automated system may not achieve these accuracies due to variable environmental conditions, projectile instability, inability to accurately estimate retardation, and larger area of coverage.

References

[1] Smith, C.L. and Li, D.G., *A forensic ballistics projectile location system*, Security Technology, 1998. Proceedings, 32nd annual 1998 International Carnahan Conference on, 12-14 Oct. 1998. Pages: 184-189.

[2] N. Levanon, *Acoustic Hit Indicator*, IEEE Trans. On Aerospace and Electronic Systems, Vol. 37 No. 1, January 2001, pp 304 - 309.

[3] N. Levanon, *Some Results from Utilizing Doppler Derivatives*, IEEE Trans. On Aerospace and Electronic Systems, Vol. AES-16 No. 5, Sept 1980, pp 727 - 724.

[4] R. J. Webster, *An Exact Trajectory Solution From Doppler Measurements*, IEEE Transactions on Aerospace and Electronic Systems, Vol. AES-18, No. 2, March 1982, pp 249 - 252.

[5] N. Levanon, S. Weinstein, *Angle-Independent Doppler Velocity Measurement*, IEEE Transactions on Aerospace and Electronic Systems, Vol. AES-19 No. 3, May 1983, pp. 354 - 359.

[6] Allen, M. R.; Stoughton, R. B.; *A Low Cost Radar Concept for Bullet Direction Finding* Proceedings of the 1996 IEEE National Radar Conference, 13-16 May 1996, pp 202-207.

[7] Armstrong, B., Holeman, B.S., *Target Tracking with a Network of Doppler Radars*, IEEE Trans. On Aerospace and Electronic Systems, Vol. 34, No. 1, January 1998.

[8] Ter Haseborg, J.L. and Trinks, H. *Detection of Projectiles by Electric Field Measurements*, IEEE Transactions on Aerospace and Electronic Systems, Vol. AES-16, No. 6, November 1980, pp 750 - 753.

[9] Moss, G.M., Leeming, D.W., Farrar, C.L., *Military Ballistics*, Brassey's Ltd., London, 1995.

TABLE I

Scoring Results At Local Range: 22 cal

22 cal Rounds	TRUTH		DARTS		ERROR		
shot	x	y	x	y	x	y	d
1	100.6	82.0	99.3	85.3	-1.3	3.3	3.5
2	99.6	84.6	99.3	87.9	-0.3	3.3	3.3
3	98.6	84.6	98.3	86.9	-0.3	2.3	2.3
4	98.0	82.3	96.3	84.1	-1.7	1.8	2.5
5	196.3	83.6	194.3	86.1	-2.0	2.5	3.2
6	197.1	74.4	195.3	76.0	-1.8	1.6	2.4
7	205.5	82.0	204.7	83.8	-0.8	1.8	2.0
8	206.5	83.1	205.5	84.8	-1.0	1.7	2.0
9	206.8	94.5	205.0	95.5	-1.8	1.0	2.1
10	205.7	101.9	204.0	103.6	-1.7	1.7	2.4
11	181.9	93.7	180.3	94.7	-1.6	1.0	1.9
				Average	-1.3	2.0	2.5
				Std. Deviation	0.6	0.8	0.6

Units of Measure: cm

TABLE II

Scoring Results At Local Range: Shotgun Slug

Shotgun Slug	TRUTH		DARTS		ERROR		
shot	x	y	x	y	x	y	d
1	99.1	92.2	97.5	94.7	-1.6	2.5	3.0
2	95.8	91.2	95.0	93.0	-0.8	1.8	2.0
3	99.3	98.8	98.3	100.3	-1.0	1.5	1.8
4	98.8	95.0	97.3	97.3	-1.5	2.3	2.7
5	194.3	86.9	193.6	89.9	-0.7	3.0	3.1
6	191.5	94.5	190.5	97.5	-1.0	3.0	3.2
7	198.4	93.2	196.9	94.2	-1.5	1.0	1.8
8	189.0	88.7	188.5	90.7	-0.5	2.0	2.1
9	195.6	72.6	193.8	75.7	-1.8	3.1	3.6
10	197.6	76.0	195.8	79.3	-1.8	3.3	3.8
11	191.3	89.2	191.0	91.7	-0.3	2.5	2.5
12	203.5	83.6	201.9	86.1	-1.6	2.5	3.0
				Average	-1.2	2.4	2.7
				Std. Deviation	0.5	0.7	0.7

Units of Measure: cm

TABLE III

Scoring Results at APG: 9 mm

9mm	TRUTH		DARTS		ERROR		
shot	x	y	x	y	x	y	d
1	67.5	94.0	67.8	93.2	0.3	-0.8	0.9
2	46.8	218.4	47.7	218.5	0.9	0.1	0.9
3	184.8	208.6	185.8	210.1	1.0	1.5	1.8
4	188.9	54.9	190.1	56.7	1.2	1.8	2.2
5	105.7	206.1	106.6	205.0	0.9	-1.1	1.4
6	160.8	173.4	161.0	172.4	0.2	-1.0	1.0
7	31.5	83.0	30.8	82.6	-0.7	-0.4	0.8
8	35.0	-33.5	34.1	-32.2	-0.9	1.3	1.6
9	-54.5	66.5	-57.6	68.0	-3.1	1.5	3.4
10	47.5	84.0	46.1	85.8	-1.4	1.8	2.3
11	47.0	71.0	45.4	72.0	-1.6	1.0	1.9
12	31.0	-20.0	30.4	-18.8	-0.6	1.2	1.3
13	24.0	-32.0	22.3	-33.5	-1.7	-1.5	2.3
				Average	-0.4	0.4	1.7
				Std. Deviation	1.3	1.2	0.8

Units of Measure: cm

TABLE IV

Scoring Results at APG: 5.56 mm

5.56mm	TRUTH		DARTS		ERROR		
shot	x	y	x	y	x	y	d
1	25.4	46.4	26.6	43.7	1.2	-2.7	3.0
2	24.3	218.8	26.2	215.6	1.9	-3.2	3.7
3	206.1	224.2	205.3	223.1	-0.8	-1.1	1.4
4	197.5	47.0	196.6	44.2	-0.9	-2.8	2.9
5	110.5	141.6	110.4	138.8	-0.1	-2.8	2.8
6	104.6	134.6	105.4	135.0	0.8	0.4	0.9
7	6.0	61.5	5.9	64.2	-0.1	2.7	2.7
8	-4.0	51.0	-3.7	52.1	0.3	1.1	1.1
9	-9.0	54.5	-8.3	56.3	0.7	1.8	1.9
10	-15.5	2.0	-16.9	1.2	-1.4	-0.8	1.6
11	-3.0	13.5	-4.5	12.9	-1.5	-0.6	1.6
12	-2.5	6.0	-3.9	8.7	-1.4	2.7	3.0
13	-3.0	3.5	-4.5	2.1	-1.5	-1.4	2.1
14	-3.5	1.0	-5.0	0.2	-1.5	-0.8	1.7
15	-8.5	-6.5	-10.8	-9.2	-2.3	-2.7	3.5
16	0.0	-10.5	-1.7	-12.5	-1.7	-2.0	2.6
17	-4.5	-12.0	-7.1	-14.8	-2.6	-2.8	3.8
18	19.0	-58.0	17.9	-56.5	-1.1	1.5	1.9
19	27.0	-61.5	25.8	-59.7	-1.2	1.8	2.2
20	38.0	-59.0	36.8	-56.2	-1.2	2.8	3.0
21	40.0	-57.0	38.9	-53.5	-1.1	3.5	3.7
				Average	-0.7	-0.3	2.4
				Std. Deviation	1.2	2.2	0.9

Units of Measure: cm

TABLE V

Scoring Results at APG: 40 mm

40mm	TRUTH		DARTS		ERROR		
shot	x	y	x	y	x	y	d
1	-11.5	-6.5	-11.4	-8.4	0.1	-1.9	1.9
2	5.2	-6.5	0.9	-6.7	-4.3	-0.2	4.3
3	-1.1	-1.1	-5.5	-1.1	-4.4	0.0	4.4
4	4.2	30.4	4.5	30.7	0.3	0.3	0.4
5	-2.1	58.6	-4.2	59.4	-2.1	0.8	2.2
6	8.4	77.0	5.0	74.3	-3.4	-2.7	4.3
				Average	-2.3	-0.6	2.9
				Std. Deviation	2.1	1.4	1.7

Units of Measure: cm

TABLE VI

Scoring Results at APG: 25 mm Type A

Type A	TRUTH		DARTS		ERROR		
shot	x	y	x	y	x	y	d
1	84.8	44.9	82.0	45.0	-2.8	0.1	2.8
2	70.0	37.6	66.7	36.4	-3.3	-1.2	3.5
3	40.6	45.7	37.9	45.0	-2.7	-0.7	2.8
4	64.1	46.4	60.3	47.4	-3.8	1.0	3.9
5	147.3	57.8	147.3	60.2	0.0	2.4	2.4
6	148.6	96.4	146.7	93.5	-1.9	-2.9	3.5
7	174.6	98.1	174.7	98.2	0.1	0.1	0.1
8	229.6	98.4	230.3	95.1	0.7	-3.3	3.4
				Average	-1.7	-0.6	2.8
				Std. Deviation	1.7	1.9	1.2

Units of Measure: cm

TABLE VII

Scoring Results at APG: 25 mm Type B

Type B	TRUTH		DARTS		ERROR		
shot	x	y	x	y	x	y	d
1	211.1	97.2	213.4	98.4	2.3	1.2	2.6
2	146.1	103.0	146.9	101.1	0.8	-1.9	2.1
3	180.7	106.8	181.1	105.9	0.4	-0.9	1.0
4	25.4	118.3	22.5	116.1	-2.9	-2.2	3.6
5	67.6	80.5	65.7	82.3	-1.9	1.8	2.6
6	64.1	101.0	63.2	102.0	-0.9	1.0	1.3
7	174.6	78.7	175.1	79.8	0.5	1.1	1.2
8	180.3	87.3	182.1	89.0	1.8	1.7	2.5
9	69.9	68.6	69.0	68.8	-0.9	0.2	0.9
				Average	-0.1	0.2	2.0
				Std. Deviation	1.7	1.5	0.9

Units of Measure: cm